INSTITUTE OF PHYSICS PUBLISHING MEASUREMENT SCIENCE AND TECHNOLOGY

Meas. Sci. Technol. **16** (2005) 1716–1729 doi:10.1088/0957-0233/16/9/003

A facility for gas- and condensed-phase measurements behind shock waves

Eric L Petersen[1], Matthew J A Rickard[2], Mark W Crofton[2], Erin D Abbey[2], Matthew J Traum[2] and Danielle M Kalitan[1]

[1] Mechanical, Materials and Aerospace Engineering, University of Central Florida, PO Box 162450, Orlando, FL 32816-2450, USA
[2] Space Materials Laboratory, The Aerospace Corporation, El Segundo, CA, USA

E-mail: petersen@mail.ucf.edu

Received 10 January 2005, in final form 8 June 2005
Published 25 July 2005
Online at stacks.iop.org/MST/16/1716

Abstract
A shock-tube facility consisting of two, single-pulse shock tubes for the study of fundamental processes related to gas-phase chemical kinetics and the formation and reaction of solid and liquid aerosols at elevated temperatures is described. Recent upgrades and additions include a new high-vacuum system, a new gas-handling system, a new control system and electronics, an optimized velocity-detection scheme, a computer-based data acquisition system, several optical diagnostics, and new techniques and procedures for handling experiments involving gas/powder mixtures. Test times on the order of 3 ms are possible with reflected-shock pressures up to 100 atm and temperatures greater than 4000 K. Applications for the shock-tube facility include the study of ignition delay times of fuel/oxidizer mixtures, the measurement of chemical kinetic reaction rates, the study of fundamental particle formation from the gas phase, and solid-particle vaporization, among others. The diagnostic techniques include standard differential laser absorption, FM laser absorption spectroscopy, laser extinction for particle volume fraction and size, temporally and spectrally resolved emission from gas-phase species, and a scanning mobility particle sizer for particle size distributions. Details on the set-up and operation of the shock tube and diagnostics are given, the results of a detailed uncertainty analysis on the accuracy of the test temperature inferred from the incident-shock velocity are provided, and some recent results are presented.

Keywords: shock tube, chemical kinetics, combustion, aerosols, shock wave, laser absorption

1. Introduction

A significant aspect of the design and analysis of devices that utilize reacting flow fields is the time-dependent interaction of the species within the high-temperature (1000 K+) combustion zone. Examples include gas turbines (Mongia *et al* 2003), internal combustion engines (Hentschel 2000), rocket nozzles (Hagemann *et al* 1998), scramjets (Curran 2001), flame synthesis of materials (Wooldridge 1998) and pulse detonation engines (Kailasanath 2003), among others. Some of the fundamental topics of importance in these applications consist of chemical kinetics, ignition and spectroscopy at high temperatures. Because of their highly repeatable test conditions and uniform flow fields, shock tubes have been used for several decades to study such topics. Details on the use of shock tubes for gas-phase combustion measurements can be found in many references, including Gaydon and Hurle (1963), Bowman and Hanson (1979), Glass and Sislan (1994), and Bhaskaran and Roth (2002).

Condensed-phase species are also present in many combustion applications and reacting flow fields including, for example, solid-propellant particles, soot particles formed within the reaction zone and liquid-propellant droplets. The general topic of heterogeneous combustion involving

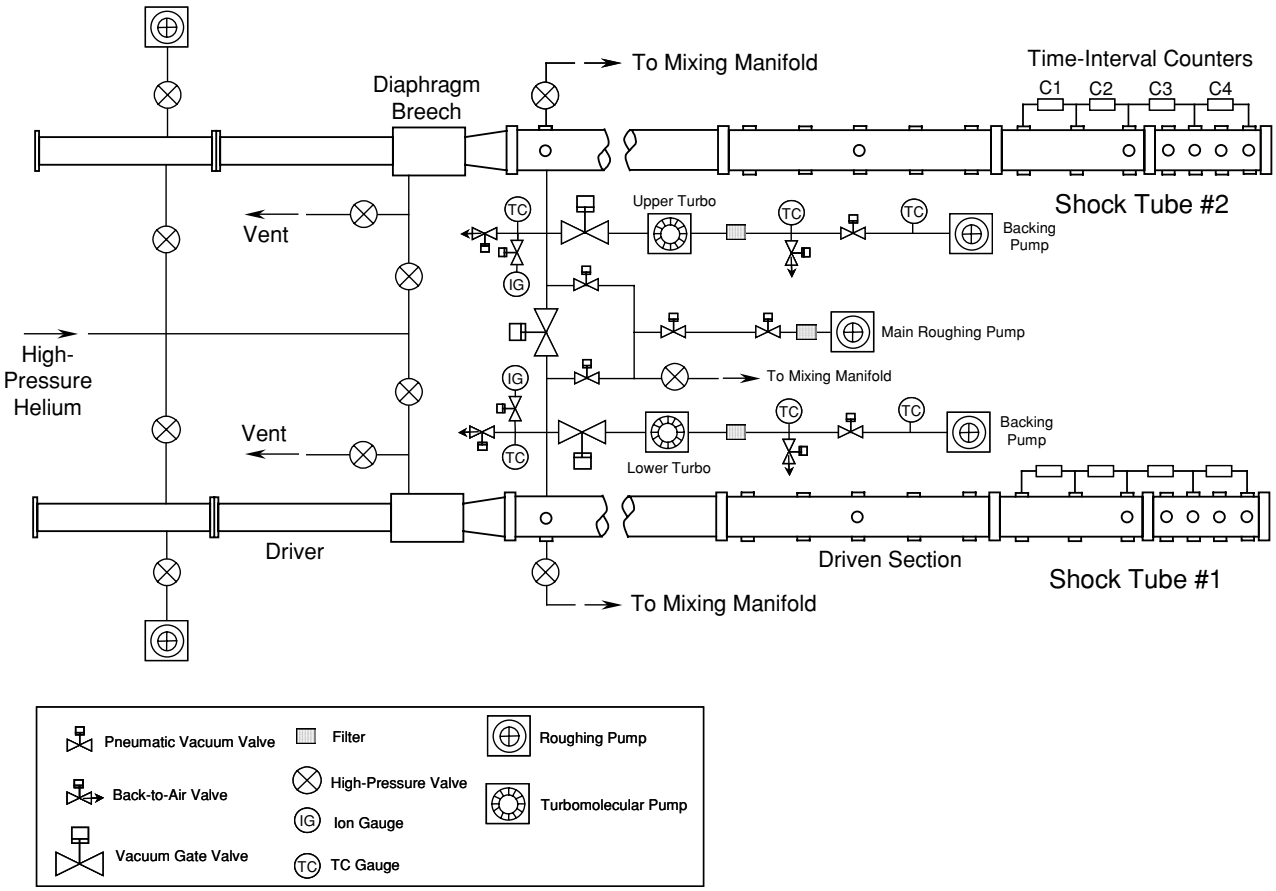

Figure 1. Shock-tube facility for gas-phase and heterogeneous combustion measurements.

gas/aerosol mixtures covers a wide range of particle sizes from a few nanometres to several millimetres. In most cases, the volume fraction of condensed species within the gas mixture is relatively low. One application of present interest is the flame synthesis of materials, wherein condensed-phase species are the desired product of a gaseous combustion process (Wooldridge 1998). Other topical applications include the study of soot formation from hydrocarbon flames (Brown *et al* 1998) and the ignition of powdered propellants (Roberts *et al* 1993).

For several years, shock tubes have been utilized for the study of heterogeneous combustion processes and the propagation of shock and detonation waves through aerosol–laden gas mixtures. Shock tubes are useful for such measurements because the shock wave can be used to heat the mixture nearly instantaneously to temperatures of the order of 1000 to 4000 K (or higher) in a controlled environment. However, shock-tube measurements in mixtures containing condensed species are generally more difficult to perform than similar measurements in purely gas-phase mixtures for several reasons, including nonideal gas-dynamic effects, optical interference from the particles and mixture nonuniformities. Some comprehensive reviews on the use of shock tubes for studying heterogeneous mixtures can be found in Nettleton (1977), Petersen (2000) and Bhaskaran and Roth (2002).

In the present application, the shock-tube technique is used to study fundamental processes related to the combustion synthesis of materials, chemical kinetics, and the ignition and oxidation of advanced propellants. The authors' facility is located at The Aerospace Corporation in El Segundo, CA. Although the basic shock-tube construction is based on the design utilized in earlier studies such as Bott and Jacobs (1969) and Bott and Cohen (1971, 1984), significant refurbishment and several upgrades were performed on the facility in recent years. In addition to facility hardware and procedural modifications, modern measurement techniques and the ability to conduct condensed-phase experiments have been implemented. This paper presents an overview of the present facility design and procedure, including specific hardware, vacuum system details and shock-velocity detection particulars. A thorough uncertainty analysis of the test-temperature error was performed, the details of which are also included. A section covering the measurement techniques and typical results specific to gas-phase combustion experiments is presented, followed by a similar overview of the diagnostics and results for condensed-phase experiments.

2. Facility design and procedure

The facility consists of the shock-tube hardware and control system, the data acquisition system, the vacuum system and the velocity detection method. Figure 1 provides a layout of the two shock tubes and a diagram of the vacuum and gas-handling systems. Both tubes are identical in design and operation, so when only a single tube is discussed in this paper it can be assumed that the content of the discussion applies

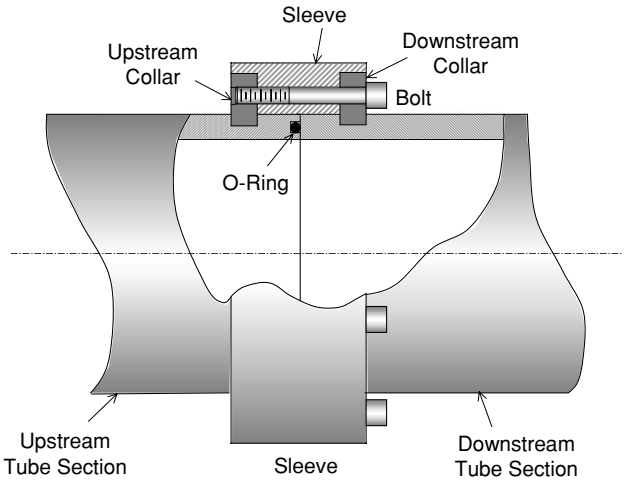

Figure 2. Weldless flange design for mating two driven-tube sections together.

to both tubes unless otherwise specified. Each of the main components is described in more detail in this section. The gas-dynamic performance of the facility is also presented.

2.1. Shock-tube hardware

Each shock tube is pressure-driven with helium and has the option of using either a single or a double diaphragm in the breech-loaded assembly (figure 1). Pre-scored aluminium diaphragms of thickness ranging from 2 to 10 mm are employed for the higher test pressures, and Lexan diaphragms ranging in thickness from 0.4 to 2 mm are utilized for test pressures $<$10 atm. A specially designed cutter located slightly downstream aids the bursting of the Lexan diaphragms. The driver section is 3.5 m (10 ft) long and has an internal diameter of 7.62 cm (3 in). The driven section has a length of approximately 10.7 m (35 ft) with an internal diameter of 16.2 cm (6.38 in). A weldless, high-pressure flange design is employed in the driven part and allows for the easy removal and addition of the segmented tube section(s) near the downstream end. Figure 2 shows the details of the flange design.

Optical and instrumentation access to the shock-heated mixture is provided by ports located at fixed intervals on the downstream section (figure 1). Further details on the port-to-port spacings are discussed in more detail in a later section. The distance between the furthest downstream port and the endwall can be varied from 1.6 cm up to 7.6 cm by using different end caps. When performing experiments with powder mixtures (described below), the distance from the reflected-shock test port to the endwall is 5.84 cm (2.3 in). The distance from the test port to the endwall is 1.6 cm when performing gas-phase chemistry experiments.

Three MKS Baratron model PDR-C-1B pressure transducers with 0–10, 0–100 and 0–1000 Torr pressure ranges are used to measure the driven-section fill pressure (P_1). Post-shock test pressures are monitored by a Kistler 603B1 piezoelectric pressure transducer using a Kistler 5010 amplifier/signal conditioner box. This Kistler pressure transducer is located in the bottom port closest to the endwall, coincident with the side-mounted optical access ports. It was found that this transducer is sensitive to heat transfer from the shocked gas, causing an artificial decay in the pressure signal with time. This problem was eliminated by placing a single layer of standard, black electrical tape on the surface of the sensor. The effect of this tape on the transducer is not significant in most experiments since the pressure reading is mostly qualitative. If absolute pressure readings are desired, the transducer signal is scaled to the post-shock conditions determined from the incident shock speed.

A computer-based data acquisition unit consisting of a Pentium computer and two computer-based oscilloscope boards from Gage Applied Sciences (one CS512 pair and one CS1602 pair) is dedicated to the shock-tube facility. The computer data acquisition unit has four channels (two per board) with a speed of at most 5 MHz per channel and 12-bit resolution. Additional data-acquisition capability is available from a two-channel, 8-bit digital oscilloscope (Tektronix TDS210).

At the time of writing, the lower shock tube (shock tube #1, figure 1) has been utilized predominantly for the experiments and applications mentioned herein. Additionally, shock tube #1 can be used as a shock tunnel by adding a test section and connecting the exhaust to an evacuated, 14.7 m^3 dump tank as in Petersen *et al* (2003). However, the use of the facility as a shock tunnel will not be covered in detail in this paper.

2.2. Vacuum system

A new vacuum system was recently implemented on the shock-tube facility. This system allows for the operation and evacuation of both shock tubes to pressures below 10^{-6} Torr after overnight pumping. When compared to the original diffusion-pump-based system, the new vacuum system design: (1) increased vacuum quality, (2) improved dependability, (3) secured modular construction and (4) incorporated flexibility and the independent, simultaneous use of both shock tubes. Figure 1 contains a schematic of the vacuum system. In the present configuration, the worst-case leak and outgassing rate is of the order of 10^{-4} Torr min^{-1}; the typical leak rate is about two–five times less than this.

The vacuum system was built around a Leybold TMP1000C (1000 l s^{-1}) turbomolecular pump (one for each tube). A Leybold D16B (450 l min^{-1}) roughing pump backs the turbomolecular pump for shock tube #2, and a Leybold D16A (400 l min^{-1}) roughing pump backs the turbomolecular pump for shock tube #1. An interface gate valve interconnects each system so that either turbomolecular pump can be used to evacuate either shock tube if needed. Both shock tubes also share a large-capacity Kinney roughing pump with the requisite isolation and interface plumbing. Not shown in figure 1 is additional plumbing that allows the primary Kinney roughing pump to serve as the backing pump for either turbomolecular pump if the need for such a configuration were to arise.

2.3. Performance

Over 1000 experiments have been performed to date with the present set-up (figure 1), encompassing reflected-shock temperatures from approximately 1000 K to greater than

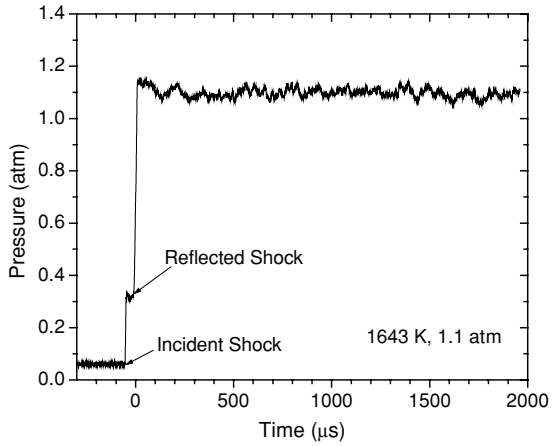

Figure 3. Typical pressure trace at the main test port located 1.6 cm from the endwall. Test gas: argon; $T_5 = 1643$ K; $P_5 = 1.1$ atm.

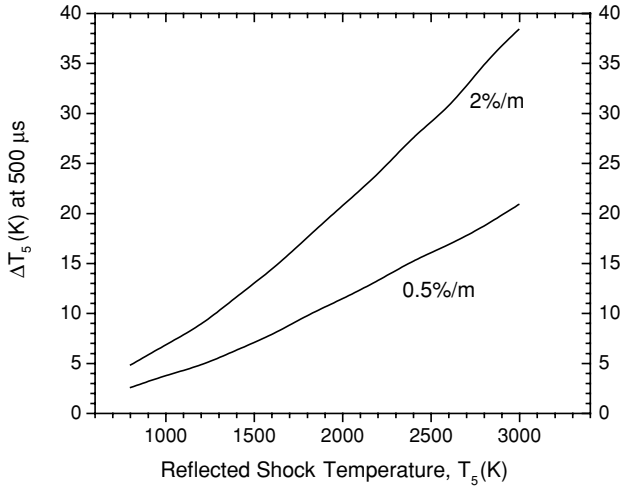

Figure 4. Predicted increase in test temperature, ΔT_5, at 500 μs past the arrival of the reflected shock wave at a port located 2 cm from the endwall for two incident-shock attenuation levels: 0.5 and 2.0% m^{-1}.

4000 K and pressures from 0.4 atm up to approximately 50 atm. All of the experiments conducted in the shock-tube facility have been done with either argon or nitrogen as the primary bath gas in the driven section. Argon is the preferred dilution gas for chemical kinetics studies because of its favourable gas dynamic properties. A typical pressure trace from an experiment in argon is shown in figure 3. The pressure is very well behaved and remains constant for the entire portion of the test time shown (2 ms) behind the reflected shock wave. From other pressure traces, it can be seen that the total test time behind the reflected shock wave in argon is about 3 ms, where the end of the test time is marked by the sudden decrease in pressure due to the arrival of an expansion wave at the test port located 1.6 cm from the endwall.

Although the pressure trace appears to be extremely uniform in time behind the reflected shock wave as predicted by ideal shock-tube theory, nonideal effects due mostly to the growth of a boundary layer behind the incident shock wave can contribute to uncertainties in the test temperature. Because of these viscous effects, the incident shock wave velocity is not constant as it traverses the tube but instead attenuates. After reflection from the endwall, the reflected shock wave then propagates into a gas mixture that is nonuniform in temperature and pressure because disturbance waves due to the boundary-layer growth and the attenuated incident shock wave tend to modify the temperatures and pressures in the tube (Mirels 1964, Petersen and Hanson 2003). The net effect is a slight increase in the temperature behind the reflected shock wave with time. The extent of this temperature (and pressure) increase is a function of the test conditions, tube diameter, and driven-section length. The adverse effects tend to be magnified by smaller-diameter tubes and higher test temperatures (i.e., higher incident-shock Mach numbers) (Petersen and Hanson 2001).

Predictions of the increase in test temperature for the facility herein were performed using the procedure and models outlined in Petersen and Hanson (2001, 2003). The results are displayed in figure 4 for a helium driver gas and argon-driven gas over a range of reflected-shock test temperatures (T_5) between 800 and 3000 K at a pressure (P_5) of 1 atm. (As is convention in shock-tube theory, the subscript 5 refers to conditions behind the reflected shock wave; the initial conditions in the driven section are denoted by 1.) Two typical incident-shock attenuations, given in terms of per cent reduction per metre of travel (i.e.,%/m), are shown; the increase in T_5 is shown as ΔT_5 at a time equal to 500 μs after passage of the reflected shock wave. The two attenuation rates, 0.5 and 2.0% m^{-1}, represent the extreme ranges of attenuation for the facility based on observation (see below).

As expected, figure 4 indicates that the increase in T_5 is greater for higher test temperatures and larger incident-shock attenuation rates. However, for the lower attenuation rate, ΔT_5 is only 11 K for an initial T_5 of 2000 K after 500 μs, or less than 0.5% of T_5. The higher attenuation rate produces a ΔT_5 of about 21 K over the same time period, or a 1% increase in T_5. Since most chemical kinetics studies are performed at temperatures less than 2000 K and occur in times less than 500 μs, the results in figure 4 demonstrate that attenuation effects are minor in the present facility for such studies. However, for experiments requiring relatively long test times (>1 ms) and very high temperatures (>2000 K), attenuation effects may not be negligible and should be considered on a case-by-case basis.

Since precise information on the shock speed is so important to the accuracy of the test results, the incident-shock velocity and its attenuation as it propagates down the driven tube must be monitored in all experiments. Corresponding increases in the pressure at the test location are not shown because the calculations indicate that they are negligible (<2%; see figure 3) and pressure effects are usually secondary to temperature effects in combustion chemistry studies. Further details on the accuracy of the shock-velocity measurements are provided in the following section.

3. Shock-velocity detection

In most experiments, it is important that the conditions behind the shock wave are known as accurately as possible, particularly the temperature. For example, when measuring a

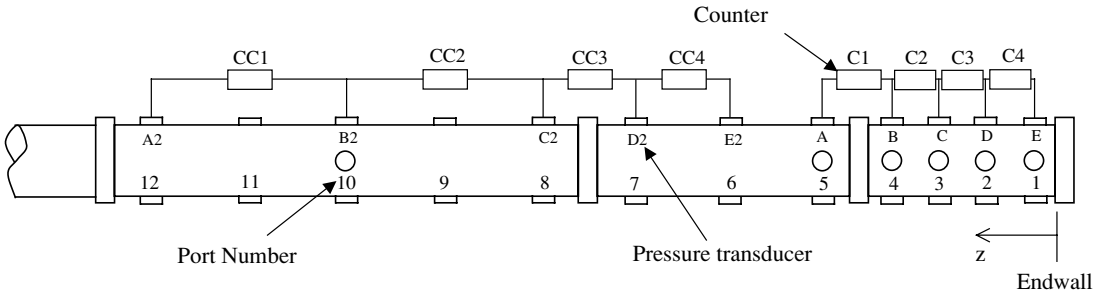

Pressure transducers

Transducer	z in (cm)	Sensitivity (mV psi^{-1})	Port #
E	2.3 (5.84)	2.65	1
D	8.3 (21.08)	2.68	2
C	14.3 (36.32)	2.75	3
B	20.3 (51.56)	2.62	4
A	30.3 (76.96)	*	5
E2	44.3 (112.5)	*	6
D2	56.3 (143.0)	*	7
C2	68.3 (173.5)	*	8
B2	92.3 (234.4)	*	10
A2	116.3 (295.4)	*	12

* Never Calibrated as a unit; should have sensitivity near PZT's B–E.

Time-interval counters

Counter	Δz in (cm)	z in (cm)
C4	6.0 (15.24)	5.3 (13.46)
C3	6.0 (15.24)	11.3 (28.70)
C2	6.0 (15.24)	17.3 (43.94)
C1	10.0 (25.40)	25.3 (64.26)
CC4	12.0 (30.48)	50.3 (127.8)
CC3	12.0 (30.48)	62.3 (158.2)
CC2	24.0 (60.96)	80.3 (204.0)
CC1	24.0 (60.96)	104.3 (264.9)

Figure 5. Locations of available ports, pressure transducers and time-interval counters on the shock-tube facility.

chemical kinetic rate coefficient with a 300 kJ mol^{-1} activation energy at 1500 K, a 1% error in temperature (i.e., 15 K) corresponds to a 25% error in the inferred Arrhenius rate. The commonly accepted approach in shock tubes is to measure the velocity of the incident shock wave and use the well-known normal-shock equations and thermodynamic properties to infer the test temperature (Gaydon and Hurle 1963). The conditions behind the reflected shock wave immediately upon reflection from the endwall depend only on the speed of the incident wave, the initial fill conditions and the known gas properties.

This method, in principle, is exact within the assumption of a normal shock wave (which is valid in most cases, particularly for the incident shock sufficiently far from the diaphragm). The underlying uncertainty, therefore, is the accuracy of the shock-velocity measurement. In an ideal scenario, the shock speed remains constant as it propagates the length of the driven section. However, nonideal effects such as viscosity, imperfect diaphragm rupture and shock acceleration due to energy release in a reactive mixture can contribute to an axially nonuniform shock speed. The axial variation in shock speed is taken into account by measuring the incident-shock velocity at multiple locations along the driven tube. Since the shock speed is not measured directly at the endwall, it is inferred from the upstream measurements by fitting a curve (usually linear) to them and extrapolating the curve to the endwall (i.e., $z = 0$).

With this in mind, a thorough analysis and characterization of the accuracy of the shock-velocity detection technique were performed. This section provides a description of the velocity-detection procedure and equipment; an error analysis on the accuracy of the velocity measurement; typical measurements; and a final, optimized configuration and procedure.

A total of ten piezoelectric pressure transducers (PCB P113A) each with a time response less than 1 μs are available to measure the shock velocity. Figure 5 contains a schematic of one of the shock tubes, showing the port, transducer and interval locations. Each transducer circuit includes a charge-to-voltage amplifier (PCB 402M148) connected to the sensor by a 1 m, low-noise, coaxial cable (PCB 003C03). The signal conditioning is accomplished by two PCB 482A18 exciter/output boxes, each with eight available channels. Transducers A–E are operated on the first five channels of one unit, and transducers A2–E2 are operated on the first five channels of the other unit. As shown in the table in figure 5, the typical sensitivity of the transducer circuits is 2.68 mV psi^{-1}. However, a 100× gain is applied to the outputs of each transducer circuit via the 482A18 units to increase their sensitivity to incident-shock passage.

Operationally, the transducers detect the rise in pressure due to the passage of the incident shock wave. The resulting voltage signals are sent to time-interval counters to time the passage of the shock wave and, hence, record the shock speed. Eight Fluke PM6666/016 counters are available. Typically, five transducers and four counters are used on one shock tube, and the same number of transducers and counters are employed on the other shock tube; for the velocity-measurement optimization experiments described herein, all of them were employed on shock tube #1.

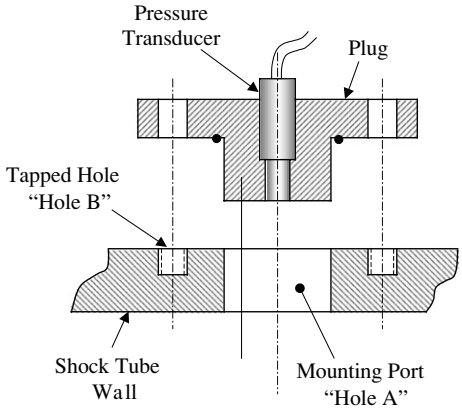

Figure 6. Pressure transducer plug and its location relative to the shock-tube sidewall.

3.1. Uncertainty analysis

When measuring the shock velocity, two quantities are needed to determine the average speed between any two locations: distance and time. These quantities relate to the known distance between the transducers and the counter measurement of the time interval. Unfortunately, there are uncertainties associated with both quantities. These uncertainties can be divided into three categories: transducer position uncertainties, transducer trigger uncertainties and counter/timer uncertainties. Typical uncertainties for each of these categories were assigned as follows, and an uncertainty analysis was performed for typical shock-tube conditions.

There are five possible sources of error associated with the machining of the ports along the shock tube and the plugs to fit those ports. Those sources are: the position and size of the large holes along the shock tube; the size of the plugs; and the position and size of the small holes within the plug. Figure 6 shows conceptually the transducer/plug assembly and its relationship to a shock-tube port. Using dial calipers that had a resolution of 0.025 mm (0.001 in), each port-to-port spacing was measured. Although it is unlikely that the total position error is even as great as 0.13 mm, it is used herein as a conservative number in the uncertainty estimates.

An uncertainty estimate associated with the triggering of the pressure transducers was based on the calibration information corresponding to each PCB pressure sensor and voltage amplifier (figure 5). In summary, the pressure transducer responds to pressure changes and produces a proportional voltage based on the sensitivity of the transducer, typically given in mV per unit of pressure. The counter/timer is triggered when the signal from the pressure transducer reaches a certain threshold voltage that is user-specified via front-panel controls. Some measurement inaccuracies arise because each transducer has a slightly different sensitivity. This means that, although each timer is triggered at the same voltage, the voltage corresponds to a slightly different pressure for each transducer.

The voltages at which the timers start and stop can be adjusted for each pressure transducer (i.e., one transducer starts the timer, and one transducer stops the timer). However, these voltages cannot be specified accurately enough to compensate for the different transducer sensitivities—the resolution of the counter/timer's input voltages is 0.02 V. For a typical pressure transducer rise of 2×10^5 V s^{-1} upon arrival of the incident shock wave, the maximum error due to trigger uncertainty for threshold trigger levels less than about 0.5 V is less than the precision of the counters themselves, or 0.1 μs. Since the threshold value is typically chosen at less than 0.5 V (around 0.26 V, or about 27% of the pressure rise for an incident shock producing a pressure of 1 atm behind the reflected shock), an uncertainty of 65 ns due to trigger errors was selected for the calculations.

Counter/timer uncertainties were based on the specifications given in the Fluke PM6666 manual. The total counter error can be divided into four sources: trigger error, time base error, systematic error and the error due to resolution. The summation of all four components equals the total error. According to the manual, the resolution for the counter/timers is 100 ns, and the systematic error for the time-interval (i.e., 'time A–B') measurements is 4 ns. The trigger error is defined as the peak-to-peak noise voltage divided by the signal slope in V s^{-1}. Pressure transducer data showed the typical noise voltage to be 0.04 V and the average signal slope to be 2×10^5 V s^{-1}. Hence, the trigger error is 200 ns per input signal. Since each timer receives two input signals (one to start the timer and one to stop it), the trigger error was doubled to 400 ns. The time base error was assumed to be 96 ns at most. Therefore, the total timing error, including the trigger error and the precision of the counters (100 ns), amounted to 665 ns for the uncertainty calculations.

Ultimately, however, the test temperature is the primary concern for most shock-tube experiments of interest herein. To this end, the uncertainty in the test temperature behind the reflected shock wave (T_5) was determined using the estimated uncertainty in the measured incident-shock velocity. For these uncertainty calculations, it was assumed that the incident-shock speed, V_s, is constant; axial attenuation of the shock wave is covered in the following section. The total errors in the shock velocity and in the test temperature were calculated using two methods: the maximum-error method and the statistical method (Holman 1994, Taylor 1982). The maximum-error method calculates the error in a function by assuming the maximum error for each of the variables in that function. The statistical method estimates the error in a function of several variables where the uncertainties in those variables are independent and random.

From the usual 1D shock-tube relations, the reflected-shock temperature is a function of the initial temperature (T_1), the gas specific heat ratio (γ) and the incident-shock Mach number, M (Gaydon and Hurle 1963):

$$T_5 = \frac{T_1[2(\gamma-1)M^2 + (3-\gamma)][(3\gamma-1)M^2 - 2(\gamma-1)]}{(\gamma+1)^2 M^2}. \tag{1}$$

It can be shown that for argon gas ($\gamma = 1.67$) and $T_1 = 300$ K, equation (1) can be approximated by

$$T_5 = 225.1M^2 + 149.85 - 74.99M^{-2}. \tag{2}$$

Equation (2) becomes useful when performing the uncertainty calculations using the statistical method. The Mach number is related to the measured shock velocity and the ideal-gas speed of sound per

$$M = \frac{V_s}{\sqrt{\gamma R T_1}} \tag{3}$$

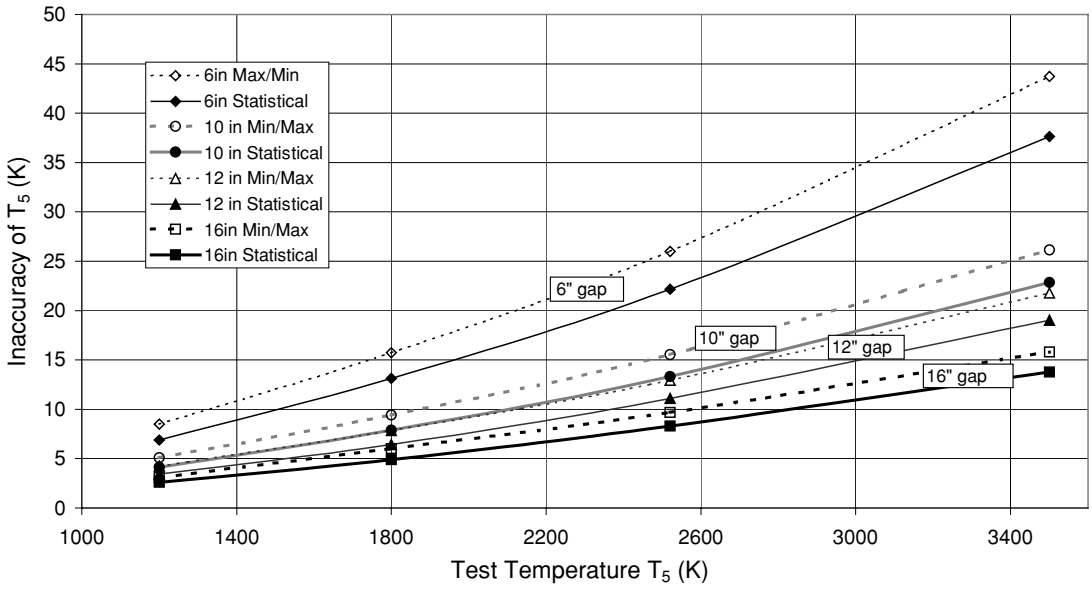

Figure 7. Calculated reflected-shock temperature (T_5) error for various transducer spacings using estimated errors in velocity-detection scheme (gas: argon).

where R is the universal ideal gas constant (8314 J kmol^{-1} K^{-1}) divided by the molecular weight and is equal to 208 J kg^{-1} K^{-1} for argon test gas. Of course, V_s is determined by the finite distance and time between pressure transducers per equation (4),

$$V_s = \frac{\Delta z}{\Delta t}. \tag{4}$$

When using the min–max error estimate, the worst-case Δz and Δt values are simply used in equations (2)–(4). However, the statistical method involves the variation of each variable that goes into the calculation of T_5 using the standard root-sum-squares (RSS) method (Holman 1994) with $V_s = V_s(\Delta z, \Delta t)$, so the uncertainty in V_s (i.e., δ_{V_s}) is obtained as

$$\delta_{V_s} = \sqrt{\left(\frac{\partial V_s}{\partial(\Delta z)}\delta_{\Delta z}\right)^2 + \left(\frac{\partial V_s}{\partial(\Delta t)}\delta_{\Delta t}\right)^2}$$
$$= \sqrt{\left(\frac{1}{\Delta t}\delta_{\Delta z}\right)^2 + \left(\frac{-\Delta z}{\Delta t^2}\delta_{\Delta t}\right)^2}. \tag{5}$$

Likewise, T_5 is only a function of M for a given test gas, so equations (2) and (3), and the RSS method give

$$\delta_{T_5} = \frac{\partial T_5}{\partial M}\delta_M = (450.19M + 149.98M^{-3})\frac{\delta_{V_s}}{\sqrt{\gamma R T_1}}. \tag{6}$$

Figure 7 provides the resulting, calculated error in T_5 for test temperatures ranging from 1200 to 3500 K and transducer spacings of 15.2, 25.4, 30.5 and 40.6 cm (i.e., 6, 10, 12 and 16 in). As expected, the min–max calculations represented by the dashed curves lead to error estimates that are more conservative than those of the statistical (RSS) method (equations (5) and (6)) which produces lower, yet more realistic, uncertainties. The effect of the transducer spacing is quite evident, where the larger spacing provides less uncertainty in the measured velocity and, hence, T_5 for the parameter ranges of this study. The uncertainty also increases with increasing test temperature.

One conclusion that can be derived from figure 7 is that the 30.5 cm spacing between the ports is better for placement of the transducers than the 15.2 cm spacing of the last four ports closest to the endwall (1–4, figure 5). Using the statistical results, the 15.2 cm spacing would lead to a T_5 error of ±13 K at 1800 K and a T_5 error of ±37 K at 3500 K. By comparison, the 30.5 cm interval reduces the errors to ±6 and ±19 K at 1800 and 3500 K, respectively. An additional benefit of a larger spacing between the ports is that the measured axial velocity profile is stretched over a greater distance and is better able to resolve the true shock attenuation (or acceleration) profile, discussed further in the following section.

3.2. Attenuation measurements and discussion

Additional uncertainty in shock velocity and, hence, test temperature comes from the axial attenuation of the incident shock wave due to nonideal effects and extrapolation of the axial velocity profile to the endwall. Several experiments were performed with the full ten-transducer, eight-counter set-up seen in figure 5.

Provided in figure 8 are typical shock-velocity measurements for three representative temperatures: 1900, 2650 and 3500 K. The axial velocity profiles in figure 8 span nearly the last 3 m of the shock tube, and the profiles are seen to be linear. The attenuation of the incident-shock velocity ranges from approximately 0.5 to 1.5% m^{-1}. A closer view of the velocity measurements for a single test is shown in figure 9 for the 3500 K case. The error bars for each point, calculated using the statistical method described above, are displayed. In general, the linear curve fit falls within the error bars of each point; this line is extrapolated to the endwall to obtain the shock velocity used to calculate T_5. If only the last four points were available for this experiment, the resulting linear fit is nearly identical to the curve fit for all eight velocities (note the dashed line in figure 9). This result is useful because only four

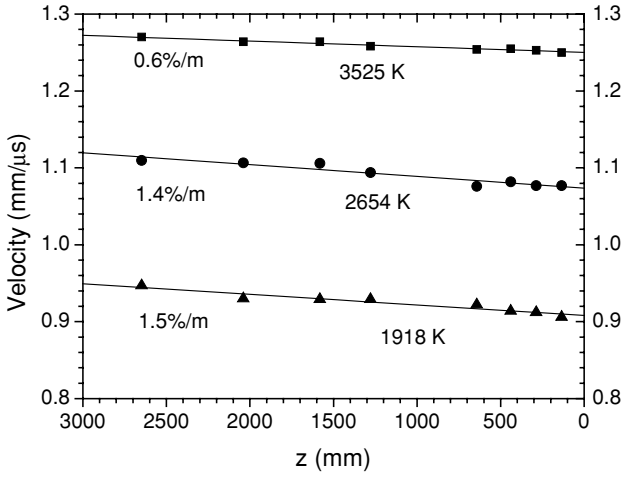

Figure 8. Sample shock-velocity measurements using the configuration in figure 5. The attenuation in % m^{-1} is given for each temperature/speed. The T_5 are based on the last velocity point.

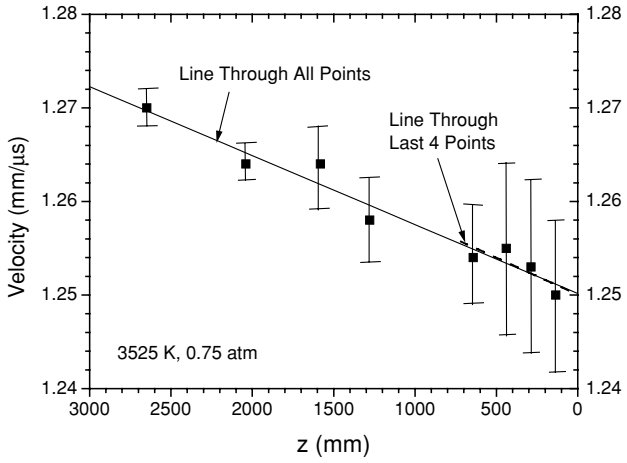

Figure 9. Detailed incident-shock velocity measurements showing error bars and curve fits. Data were taken using the set-up in figure 5.

points will be available in most shock-tube experiments when both shock tubes are operated simultaneously.

Since only five transducers and four counters are available on either Aerospace shock tube for a given experiment, their optimum location is of interest from the standpoint of minimizing the uncertainty in the reflected-shock test temperature. From the preceding calculations and results, one conclusion is that a larger spacing between transducers is preferred to reduce the velocity error, as expected. However, one limitation is the port-to-port spacing currently available on the shock tube(s) as shown in figure 5. The spacing is fixed and is not always uniform over the last 3 m. Another limitation is that the velocity-measurement points should be as close to the endwall as possible because the velocity closest to the endwall is of most interest, chiefly because the shock propagation may be, in rare instances, non-monotonic. Nonetheless, figure 8 indicates that the typical axial velocity profile is usually linear over the last 3 m.

An acceptable compromise is the final configuration in figure 10. This set-up provides two 30.5 cm intervals, one 35.6 cm interval and one 40.6 cm interval. The corresponding T_5 uncertainties for each interval are as shown in figure 7. Typical results using the suggested set-up (figure 10) are provided in the three graphs in figure 11. In these experiments, the extra transducers and counters were configured in parallel with the primary instruments to check their trigger and sensitivity characteristics. The primary set of transducers (A–E) and counters (C1–C4) is referred to as set A, and the secondary set of transducers (A2–E2) and counters (CC1–CC4) is referred to as set B.

Figure 11(*a*) presents a case wherein the velocity points clearly follow a linear trend that is well within the expected uncertainty of each velocity measurement. Additionally, both sets of velocity data agree within the expected uncertainty of each point and, most importantly, the extrapolated endwall velocity for each leads to test temperatures that are within 8 K of each other (i.e., within 0.4% of the absolute value of T_5). One conclusion from figure 11(*a*) is that linearly extrapolating the velocity to the endwall is better than simply using the last velocity point, which overestimated T_5 by 17 K for both sets. However, if the only recourse is to use the last counter time to estimate the endwall velocity—such as for rare trigger failures, etc—the estimate for T_5 is still within 1% of the expected value for the conditions of figure 11(*a*).

The error in test temperature derived using only the last velocity point should reduce when the last interval is moved closer to the endwall, as is the case in chemical kinetics experiments. Calculations using a 1.6 cm spacing between the last port (#1, figure 5) and the endwall indicate that the T_5 error using only the last interval is approximately half of the error shown in figure 11, where the last port (transducer E) is 5.84 cm from the endwall.

Occasionally, the four velocity points appear highly nonlinear, as shown in figures 11(*b*) and (*c*). Although both sets A and B provided velocities that differ from one another within the expected uncertainty of the measurements, the anomalous points differ from a linear curve fit by values greater than the expected uncertainty. The exact cause of non-monotonic results such as those seen in figures 11(*b*) and (*c*) is not known at this time but may be attributed to a secondary nonideal shock formation/propagation effect or vibration that perturbs the trigger signal(s). Such variation in the shock speed from linearity actually shows up in the velocity data when taken over a longer distance as in figure 8, but they are minimal when compared to the overall curve fit. Therefore, a linear fit through the last four points regardless of their appearance seems reasonable in light of the overall attenuation trends. This approach is supported by the T_5 results displayed in figures 11(*b*) and (*c*) (and figure 9), where linear extrapolation to the endwall for both sets A and B leads to temperatures that agree within 0.1–0.3% of each other. Additionally, the use of the last velocity measurement to infer the endwall velocity leads to test temperatures that differ from the linearly extrapolated values by only 0.2–0.6%. The conclusion here is that some scatter in the velocity measurement (as in figure 11(*b*)) does not pose a significant degradation in the accuracy of the endwall velocity when compared to the overall accuracy of each individual velocity measurement.

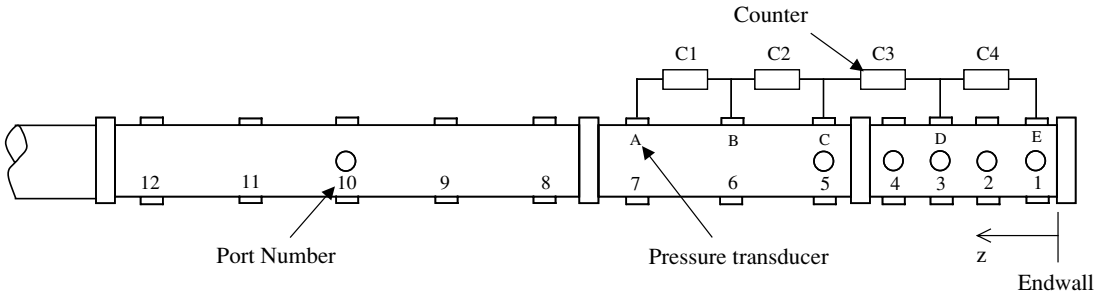

Pressure transducers

Transducer	z in (cm)	Port #
E	2.3 (5.84)	1
D	14.3 (36.32)	3
C	30.3 (76.96)	5
B	44.3 (112.52)	6
A	56.3 (143.00)	7

Time-interval counters

Counter	Δz in (cm)	z in (cm)
C4	12.0 (30.48)	8.3 (21.08)
C3	16.0 (40.64)	22.3 (56.64)
C2	14.0 (35.56)	37.3 (94.74)
C1	12.0 (30.48)	50.3 (127.8)

Figure 10. Final location of pressure transducers and counters for future experiments.

4. Gas-phase chemistry measurements

A major application of the shock-tube facility is the study of high-temperature chemical kinetics, ignition chemistry and spectroscopy in gas-phase mixtures highly diluted in a bath gas, usually argon. The diagnostics of choice herein for making detailed measurements of gas-phase species concentrations are primarily non-intrusive, optical techniques. Two methods in particular, absorption and emission, are available to monitor the behaviour of species such as OH, CH, SiH_2 and SiH_4 (Petersen *et al* 2003, Petersen and Crofton 2003, Rickard *et al* 2005), among others. A brief summary of each technique and some typical results are provided as follows.

Laser absorption spectroscopy such as in Hanson (1977) has been a common optical diagnostic technique in shock tubes for over 25 years. In this method, the transmitted laser intensity through the shock tube test section, I, is related to the incident intensity, I_0, through Beer's law:

$$\frac{I}{I_0} = \exp(k_\nu PXL), \tag{7}$$

where k_ν is the absorption coefficient of the species of interest at frequency ν, P is the total pressure, X is the absorbing species mole fraction, and L is the path length (i.e., the shock-tube inner diameter).

A schematic of the technique as utilized on the present facility for the measurement of an A–X transition of SiH_2 at 17 260.82 cm^{-1} is presented in figure 12. A Coherent 699-21 ring-dye laser operating on Rhodamine 590 dye, pumped by all lines of a Coherent Innova I-20 argon-ion laser, is the tunable light source. A sample of the beam is sent to a Burleigh WA-4500 wavemeter to monitor the frequency with a resolution of 0.01 cm^{-1}, and the main beam is focused through the CaF_2 windows in the shock tube to a diameter of the order of 1 mm. Both I_0 and I are monitored by New Focus Model 2031 Si photodiodes with a 1 MHz bandwidth. A differential preamplifier (SRS SR560) is used to take the differential absorption signal, $I_0 - I$, and this difference signal along with I_0 are sent to separate channels on a computer-based oscilloscope described in section 2.1. Additionally, a second Coherent 699–21 ring-dye laser is available, as is a Coherent solid-state pump laser (Verdi V8, 532 nm).

Another diagnostic based on laser absorption is the frequency modulation (FM) laser absorption spectroscopy set-up for shock-tube measurements of high-temperature, gas-phase kinetics. This technique is capable of resolving species concentrations ten or more times lower than what can be measured using standard differential laser absorption (Votsmeier *et al* 1999). Additionally, the FM laser absorption technique is virtually insensitive to interference absorption and scattering due to particle formation and flow field turbulence because it operates only at frequencies of the order of the spectroscopic transition. Further details are provided in Crofton and Petersen (2005).

Figure 13 contains a typical absorption time history when the FM laser absorption diagnostic is applied to the measurement of SiH_2 near 579 nm in comparison with a coincident differential absorption measurement. The profiles in figure 13 are from a mixture of 500 ppm SiH_4 shock heated to 1552 K and 1.1 atm; the silane quickly decomposes to form SiH_2 and H_2, the former of which is measured as shown. At the conditions of the FM absorption trace in figure 13, soot particles of Si_xH_y compounds are formed at later times and are quite apparent in the differential measurement but do not cause interference to the FM absorption signal because the technique is insensitive to the particles, as mentioned above.

A complementary optical diagnostic and one much easier to apply is the monitoring of emission from key molecules in the post-shock reaction zone. Since the total emission is proportional to the number density of the emitting molecules, the emission time histories are indications of when a species is formed or depleted and how much is present. Discrimination between species and background emission can be obtained by monitoring the emission at narrowband wavelengths

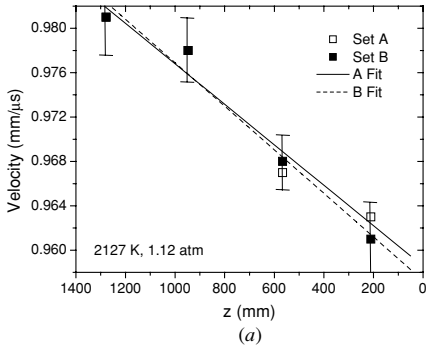

T_5 (K)	Set A	Set B
Line	2127	2119
Last Pt.	2144	2136

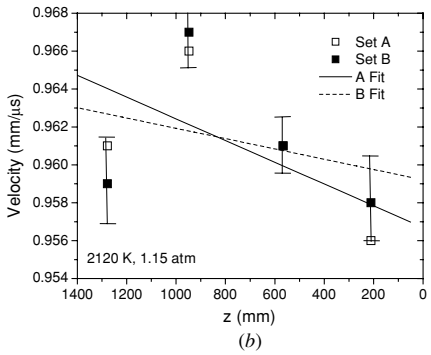

T_5 (K)	Set A	Set B
Line	2120	2128
Last Pt.	2116	2124

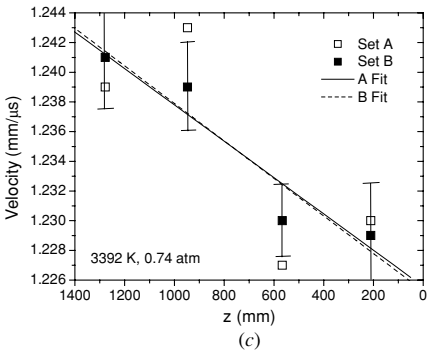

T_5 (K)	Set A	Set B
Line	3392	3387
Last Pt.	3414	3408

Figure 11. Typical shock-velocity measurements using the optimized set-up suggested in figure 10. Two sets of transducers/counters were employed; set A used transducers A–E and counters C1–C4; set B used transducers A2–E2 and counters CC1–CC4. T_5 was calculated using both linear extrapolation of the lines to the endwall and the last velocity point. (*a*) Near-linear example; 2127 K, 1.12 atm; error bars correspond to set B; att = 1.88% m^{-1}. (*b*) Example with nonlinearity; 2120 K, 1.15 atm; error bars correspond to set B; att = 0.6% m^{-1}. (*c*) Example with nonlinearity; 3392 K, 0.74 atm; error bars correspond to set B; att = 1.03% m^{-1}.

corresponding to a characteristic electronic or rotational–vibrational transition.

In general, the gas-phase emission measurements are performed by focusing the emitted light using a mirror through a shock-tube port and onto a fast-response detector. Narrowband filters, typically ±10 nm, are selected to coincide with the desired spectroscopic transition. When the emitted radiation is in the visible or ultraviolet, the emission detectors consist of photomultiplier tubes (PMTs). The PMT detectors are either 1P21 or 1P28 tubes from Hamamatsu mounted in homemade housings, powered by a Hamamatsu C3830 HV power supply. Great care was taken to optimize the signal-to-noise (S/N) ratio, time response (<2 μs), and linearity of these PMT detectors. When the emitted radiation is in the infrared, a pair of Judson InSb detectors, model J10D-M204-R01M-60, with matched amplifiers (model PA-9), a 1 mm element, and a 900 kHz bandwidth are employed.

Most measurements are usually made from a sidewall location to obtain a temporally resolved species profile. Endwall emission measurements are also performed when only ignition delay time information is required from fuel/oxidizer mixtures, but such traces are not generally useful for times after the initial ignition. Emission diagnostics applied to the present facility include SiH_4 IR emission at 4.7 μm (Petersen and Crofton 2003), OH^* chemiluminescence at 307 nm (Kalitan *et al* 2004) and CH^* chemiluminescence at 430 nm (Petersen *et al* 2004). The OH^* and CH^* diagnostics are convenient for the measurement of ignition delay times of fuel/oxidizer mixtures. Figure 14 shows two simultaneous CH^* measurements—one from the sidewall and one from the endwall—during the ignition of an $C_2H_2/O_2/SiH_4/Ar$ mixture (Rickard *et al* 2005). As mentioned above, the temporal features of the excited-state CH formation and quenching are clearly resolved in the sidewall measurement, while the endwall measurement only resolves the initial rise at ignition. It should be noted that emission from gas-phase species can also be performed in experiments containing powders and other condensed particles as described in the following section.

5. Condensed-phase measurements

Due to their versatility and highly repeatable test conditions, shock tubes are also employed for the study of heterogeneous combustion phenomena. Two main types of heterogeneous studies have been designed and implemented with the present facility: (1) the vaporization of powdered aerosols; and (2) the formation of soot particles from the gas phase. The technical details of seeding aerosols into the flow field are discussed below, and the diagnostics available for both types of heterogeneous experiments are presented.

Over the past four decades, several techniques have been utilized to uniformly disperse a solid powder into the driven section of a shock tube. A thorough review of these techniques is provided in Petersen (2000). Among the most popular methods are: (1) those which utilize the induced gas flow behind the incident shock wave to disperse a sample of powder placed within the shock tube; (2) those which premix the powder with the gas and quickly fill the shock tube a few seconds prior to running a test; and (3) those which employ a steady flow system that blows the gas/particle mixture through the test section prior to an experiment.

The technique initially chosen for the present work is one that involves incident-shock dispersion of a powder sample. This method was selected for the first experiments for several reasons, including its ease of use, short set-up time, and reasonably established dispersion characteristics (Seeker *et al* 1980). Figure 15 presents a conceptual view of the powder-dispersion technique. A sample of the powder is placed at the centre of a thin (3 mm) steel plate that spans the shock-tube internal diameter. This plate is located 15.2 cm (6 in) upstream of the primary test port and, subsequently, 21.0 cm

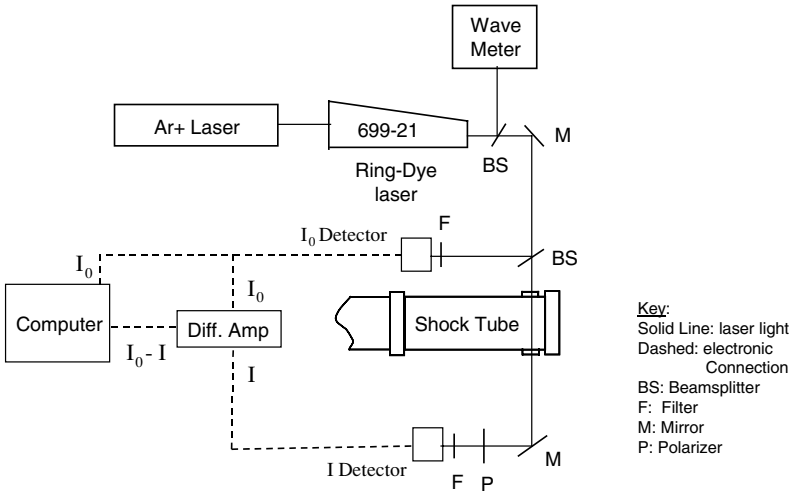

Figure 12. Differential laser absorption set-up for monitoring SiH_2 at 579 nm.

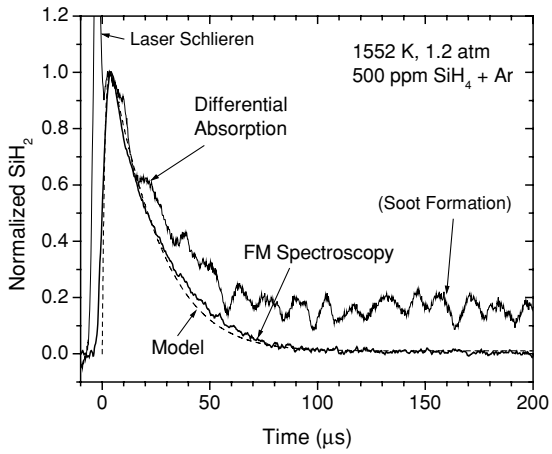

Figure 13. Typical FM spectroscopy and differential laser absorption measurement of SiH_2 from the pyrolysis of 500 ppm SiH_4 in argon behind a reflected shock wave at 1552 K and 1.2 atm. Soot formation is picked up in the differential absorption but not the FM technique.

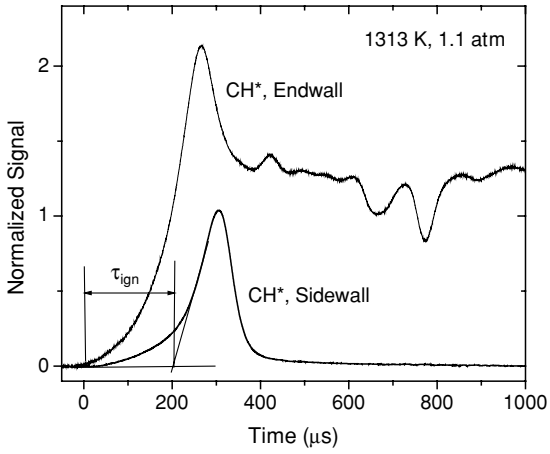

Figure 14. Sample emission measurements of CH* chemiluminescence for a 0.57% C_2H_2 + 1.43% O_2 + 0.035% SiH_4 + 97.96% Ar mixture at 1313 K and 1.1 atm. Time zero is relative to the arrival of the reflected shock wave at the sidewall measurement location.

upstream of the endwall. As seen in figure 15, the relative locations of the powder sample, endwall, and test port are critical to the timing of the experiment. The particles accelerate nearly instantaneously to the flow speed behind the incident shock wave and must reach the test section before the reflected shock wave arrives. Although this dispersion method is relatively simple to employ, inevitable spatial and temporal nonuniformities exist in the gas/particle mixture due to the nonideal nature of the mixing. At the time of writing, alternative methods are being considered for introducing a solid powder into the test-gas mixture.

Several non-intrusive optical diagnostic techniques are currently employed for making measurements in shock-heated gas/particle mixtures. Figure 16 details the applicable diagnostics currently in use on the shock-tube facility. Among these are temporally resolved emission at a single wavelength (discussed previously), multi-wavelength emission using a spectrometer and laser extinction. Also available is a separate system for measuring the particle size distribution of powder samples.

Spectrally resolved information can be obtained from the gas-phase species emission after the particles have vaporized by collecting the radiation with a spectrometer. Such measurements are useful for gross identification of species within the reaction zone when temporal resolution is not a concern. Light emitted from the gas/particle reaction zone is taken from the endwall of the shock tube and directed onto the collimating mirror of the spectrometer (figure 16). The spectrometer is a 1 m GCA/McPherson model 2051. The grating is replaceable and is chosen to optimize the wavelength range/species of interest. In general, the light is collected by a ccd camera, the output of which returns a time-integrated signal that corresponds to the total light collected for the duration of the experiment. The camera employed is a Roper Scientific IMAX512 with a UV-sensitive, 512 × 512 array. This camera is intensified and controlled by a ST-133 DMA controller and SRS DG535 digital delay generator, so some discrimination can be made as to the time interval the camera records data by controlling the intensifier gate.

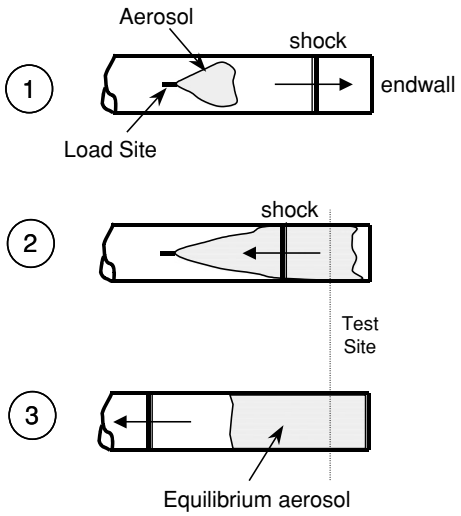

Figure 15. Particle dispersion technique. The flow behind the incident shock wave is used to blow and disperse the particles towards the test port, prior to arrival of the reflected shock wave.

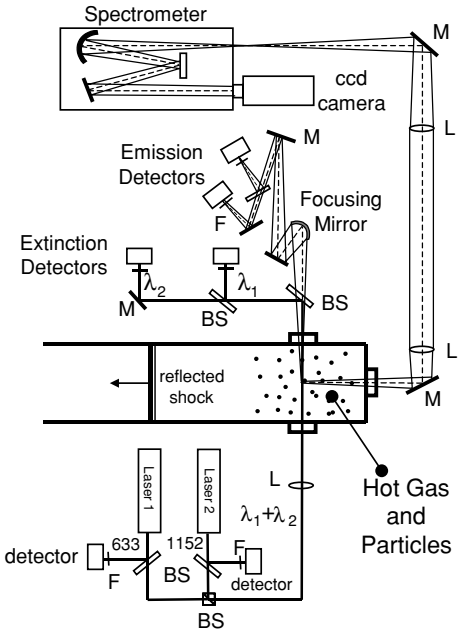

Figure 16. Optical diagnostic set-up for performing measurements in gas/particle mixtures. The diagnostics include time-resolved emission, spectrally resolved emission (spectrometer), and laser extinction at two different wavelengths.

Presented in figure 17 is a typical emission measurement using the spectrometer diagnostic in a TiO_2 decomposition experiment at a reflected-shock temperature of 4440 K and pressure of 0.5 atm (Petersen and Welle 2001). The TiO_2 powder sample was placed on the plate within the shock tube and dispersed as described above and in figure 15. The key intermediate species TiO was monitored in this experiment, so the grating was chosen to observe an 80 nm wavelength range centred on the TiO C–X spectroscopic transition near 530 nm.

One established method for monitoring the presence of submicron particles in the reaction zone is laser extinction. By passing a laser beam through a gas/particle mixture, the

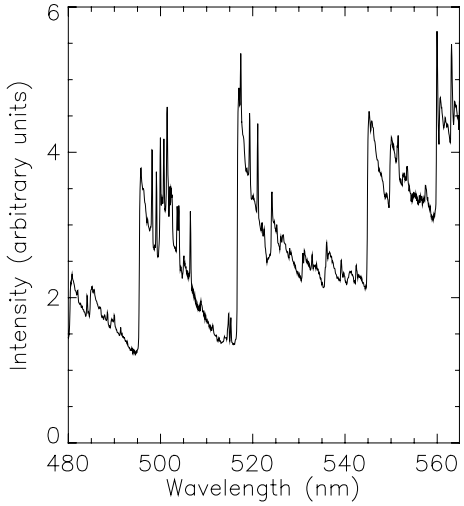

Figure 17. Sample spectrometer data for TiO C–X emission. Test conditions: TiO_2 powder in argon; 4440 K, 0.5 atm.

ratio of the transmitted to incident radiation is related to the average number density of the particles and the optical characteristics of the particles via the Bouger–Lambert law (Siegel and Howell 1992):

$$I/I_0 = \exp(-K_e L) = \exp(-N\sigma_e L) \tag{8}$$

where K_e is the extinction coefficient (cm^{-1}), L is again the path length (cm), N is the particle number density (particles cm^{-3}), and σ_e is the extinction cross section per particle (cm^2).

If the extinction properties of the particles are known at the wavelength and temperature of the experiment, the volume fraction of the particles can be measured as a function of time. Typically, Mie theory is applied in the calculations, and if the average particle diameter, d, is much smaller than the wavelength of the light, λ ($d \ll \lambda/\pi$), the Rayleigh approximation to the Mie theory can be applied (Kellerer *et al* 1996). By utilizing two wavelengths simultaneously, both the particle size and number density can be measured via the dispersion quotient method (Wittig *et al* 1981).

The present set-up, shown in figure 16, utilizes two HeNe laser beams of different wavelength (633, 1152 nm). Photodiode detectors are used to measure the incident and transmitted light. Detectors employed for this purpose include the New Focus 2031 and/or 2032 and the Electro-Optics Technology, Inc. (EOT) ET-2040 Si-photodiode models for the UV and visible laser wavelengths; the IR wavelengths are monitored with InGaAs detectors from EOT, model ET-3020. The differential extinction signals are obtained using an SRS SR560 differential preamplifier.

Figure 18 presents a representative laser extinction measurement of carbon soot formation in a fuel-rich toluene/O_2/Ar mixture. The results are displayed in the form of the soot yield, Y, as a function of time. Using equation (8), the yield Y can be calculated from the extinction measurement via

$$Y = \frac{[c]}{[c]_{\text{total}}} = \frac{\ln(I_0/I)}{\sigma_e L [c]_{\text{total}}}. \tag{9}$$

The value used for the extinction cross section was $\sigma_e = 6.6 \times 10^{-19}$ cm^2 per the data of Rawlins *et al* (1984); $[c]$ represents

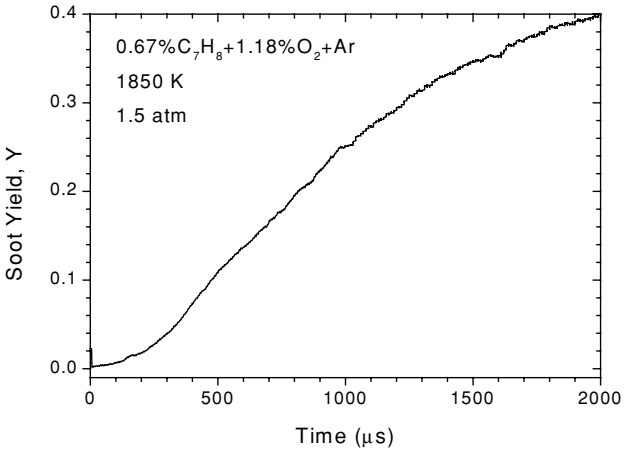

Figure 18. Laser extinction measurement of the soot yield in a 0.67% C_7H_8/1.18% O_2/argon mixture. Fuel/O_2 equivalence ratio = 5.09; 1850 K, 1.5 atm; $\lambda = 633$ nm.

the concentration of carbon atoms measured, and $[c]_{\text{total}}$ is the total concentration of carbon atoms from the initial fuel concentration. The extinction measurement of figure 18 was obtained using only the 633 nm laser wavelength.

An important aspect of the solid-phase measurements, particularly for data analysis and interpretation, is the size distribution of the powder introduced into the shock tube. Similar information is also important for analysing the size characteristics of particles formed from gas-phase chemistry within the shock tube and in other experiments. To satisfy these requirements, a Model 3936 scanning mobility particle sizer (SMPS) from TSI is utilized. This model of the SMPS is capable of measuring the number of particles in discrete size ranges from 10 to 1000 nm. The net result is a histogram of the powder sample's particle-size distribution. Perhaps the most difficult issue with measuring the size distribution of submicron solid particles is the breaking up of the inevitable agglomerations into the fundamental particles. At present, a disperser similar to that of Rajathurai *et al* (1990) is employed.

6. Summary

A recently refurbished and outfitted shock-tube facility consisting of two identical shock tubes for the study of gas- and condensed-phase combustion was described. Among the upgrades to the facility were a new high-vacuum system, gas-handling and control electronics, a diaphragm cutter assembly for lexan diaphragms, a computer-based data acquisition system and techniques for the study of gas/particle mixtures. Since the measurement of the incident-shock velocity is crucial to the accuracy of the inferred test temperature, a thorough uncertainty analysis was performed. The results of the uncertainly analysis indicate that the final interval spacing and the extrapolation of the measured axial velocity to the endwall maintain the uncertainty in the initial reflected-shock temperature to less than 10 K at 1800 K and about 20 K at 3500 K. Additional calculations that take into account the nonideal viscous effects indicate the temperature change after initial shock reflection should be minimal for conditions expected of chemical kinetics experiments.

Non-intrusive optical diagnostics available for the measurement of gas-phase species concentrations include differential laser absorption, FM laser absorption spectroscopy and narrowband emission. Spectrally resolved emission is also available using a spectrometer, and a laser extinction technique has been employed to measure the time-dependent growth of solid particulates from gas-phase reactions. Measurements performed to date include the ignition of fuel/oxidizer mixtures, the evaluation of chemical kinetic rate coefficients, the study of solid particle vaporization, and the fundamental formation of soot particles from the gas phase.

Acknowledgments

This work was supported by The Aerospace Corporation for the Air Force Space and Missile Systems Center under contract no F04701-00-C-0009. The authors acknowledge the support of Dr Ronald Cohen and assistance from Carrol Gardner, Dr Richard Welle, Thomas Baldwin, Thomas Albright, Gary Harper, Earnest Yhonsee, and William Hansen during the fabrication, set-up, and operation of the facility described herein. Additional support was provided through an AF SBIR subcontract from GE-EERC (Irvine, CA) with Dr Vladimir Zamansky and Dr Vitali Lissianski as monitors.

References

Bhaskaran K A and Roth P 2002 The shock tube as wave reactor for kinetic studies and material systems *Prog. Energy Combust. Sci.* **28** 151–92

Bott J F and Jacobs T A 1969 Shock-tube studies of sulfur hexafluoride *J. Chem. Phys.* **50** 3850–5

Bott J F and Cohen N 1971 Shock-tube studies of HF vibrational relaxation *J. Chem. Phys.* **55** 3698–706

Bott J F and Cohen N 1984 A shock-tube study of the reaction of the hydroxyl radical with propane *Int. J. Chem. Kinet.* **16** 1557–66

Bowman C T and Hanson R K 1979 Shock tube measurements of rate coefficients of elementary gas reactions *J. Phys. Chem.* **83** 757–63

Brown N J, Revzan K L and Frenklach M 1998 Detailed kinetic modeling of soot formation in ethylene/air mixtures reacting in a perfectly stirred reactor *Proc. Combust. Inst.* **27** 1573–80

Crofton M W and Petersen E L 2005 Frequency modulation spectroscopy in a particle-forming environment for the detection of SiH_2 *Proc. Combust. Inst.* **30** 1583–9

Curran E T 2001 Scramjet engines: the first forty years *J. Propul. Power* **17** 1138–48

Gaydon A G and Hurle I R 1963 *The Shock Tube in High-Temperature Chemical Physics* (New York: Reinhold)

Glass I I and Sislian J P 1994 *Non Stationary Flows and Shock Waves* (Oxford: Clarendon)

Hagemann G, Immich H, Nguyen T V and Dumnov D E 1998 Advanced rocket nozzles *J. Propul. Power* **14** 620–34

Hanson R K 1977 Shock tube spectroscopy: advanced instrumentation with a tunable infrared diode laser *Appl. Opt.* **16** 1479–81

Hentschel W 2000 Optical diagnostics for combustion process development of direct-injection gasoline engines *Proc. Combust. Inst.* **28** 1119–35

Holman J P 1994 *Experimental Methods for Engineers* 6th edn (New York: McGraw-Hill)

Kailasanath K 2003 Recent developments in the research on pulsed detonation engines *AIAA J.* **41** 145–59

Kalitan D M, Rickard M J A, Hall J M and Petersen E L 2004 Ignition measurements of ethylene–oxygen-diluent mixtures with and without silane addition *AIAA Paper* 2004-1323

Kellerer H, Müller A, Bauer H-J and Wittig S 1996 Soot formation in a shock tube under elevated pressure conditions *Combust. Sci. Tech.* **113–114** 67–80

Mirels H 1964 Shock tube test time limitation due to turbulent-wall boundary layer *AIAA J.* **2** 84–93

Mongia H C, Held T J, Hsiao G C and Pandalai R P 2003 Challenges and progress in controlling dynamics in gas turbine combustors *J. Propul. Power* **19** 822–9

Nettleton M A 1977 Shock-wave chemistry in dusty gases and fogs: a review *Combust. Flame* **28** 3–16

Petersen E L 2000 Shock tube measurements of heterogeneous combustion phenomena *Spring 2000 Meeting* (*Western States Section of the Combustion Institute*) Paper No. 00S-45

Petersen E L and Crofton M W 2003 Measurements of high-temperature silane pyrolysis using SiH_4 IR emission and SiH_2 laser absorption *J. Phys. Chem.* A **107** 10988–95

Petersen E L and Hanson R K 2001 Nonideal effects behind reflected shock waves in a high-pressure shock tube *Shock Waves* **10** 405–20

Petersen E L and Hanson R K 2003 Improved turbulent boundary-layer model for shock tubes *AIAA J.* **41** 1314–22

Petersen E L, Kalitan D M and Rickard M J A 2004 Reflected shock ignition of $SiH_4/H_2/O_2/Ar$ and $SiH_4/CH_4/O_2/Ar$ mixtures *J. Propul. Power* **20** 665–74

Petersen E L, Rickard M J A and Welle R P 2003 High-temperature nonreacting flow fields generated by a hypersonic chemical laser nozzle *J. Thermophys. Heat Transfer* **17** 420–2

Petersen E L and Welle R P 2001 Studies on single- and two-component nanoparticle decomposition using a shock tube *23rd Int. Symp. on Shock Waves* Paper No. 2376

Rajathurai A M, Roth P and Fissan H 1990 A shock and expansion wave-driven powder disperser *Aerosol Sci. Tech.* **12** 613–9

Rawlins W T, Cowles L M and Krech R H 1984 Spectral signatures (0.2–5 μm) of soot initiation in the pyrolysis of toluene near 2000 K *Proc. Combust. Inst.* **20** 879–86

Rickard M J A, Hall J M and Petersen E L 2005 Effect of silane addition on acetylene ignition behind reflected shock waves *Proc. Combust. Inst.* **30** 1915–23

Roberts T A, Burton R L and Krier H 1993 Ignition and combustion of aluminum/magnesium alloy particles in O_2 at high pressures *Combust. Flame* **92** 125–43

Seeker W R, Lester T W and Merklin J F 1980 Shock tube techniques in the study of pulverized coal ignition and burnout *Rev. Sci. Instrum.* **51** 1523–31

Seigel R and Howell J R 1992 *Thermal Radiation Heat Transfer* 3rd edn (Washington, DC: Hemisphere)

Taylor J R 1982 *An Introduction to Error Analysis* (Sausalito, CA: University Science Books)

Votsmeier M, Song S, Davidson D F and Hanson R K 1999 Sensitive detection of NH_2 in shock tube experiments using frequency modulation spectroscopy *Int. J. Chem. Kinet.* **31** 445–53

Wittig S L K, Zahoransky R A and Sakbani Kh 1981 The dispersion quotient technique in submicron particle size analysis *J. Aerosol Sci.* **12** 183–4

Wooldridge M A 1998 Gas-phase combustion synthesis of particles *Prog. Energy Combust. Sci.* **24** 63–87